ELSEVIER

Materials Science and Engineering A 474 (2008) 342–347

MATERIALS SCIENCE & ENGINEERING A

www.elsevier.com/locate/msea

Evolution of defect structures during cold rolling of ultrafine-grained Cu and Cu–Zn alloys: Influence of stacking fault energy

Y.H. Zhao [a], Z. Horita [b], T.G. Langdon [c,d], Y.T. Zhu [a,*]

[a] *Materials Physics and Applications Division, Los Alamos National Laboratory, MS G755, Los Alamos, NM 87545, USA*
[b] *Department of Materials Science & Engineering, Faculty of Engineering, Kyushu University, Fukuoka 819-0395, Japan*
[c] *Department of Aerospace & Mechanical Engineering, University of Southern California, Los Angeles, CA 90089-1453, USA*
[d] *Mork Family, Department of Chemical Engineering and Materials Science, University of Southern California, Los Angeles, CA 90089-1453, USA*

Received 4 October 2006; received in revised form 3 April 2007; accepted 8 June 2007

Abstract

Samples of pure Cu, bronze (Cu–10 wt.% Zn) and brass (Cu–30 wt.% Zn) with stacking fault energies (SFE) of 78, 35, and 14 mJ/m^2, respectively, were processed by high-pressure torsion (HPT) and by a combination of HPT followed by cold-rolling (CR). X-ray diffraction measurements indicate that a decrease in SFE leads both to a decrease in crystallite size and to increases in microstrain, dislocation and twin densities for the HPT and HPT + CR processed ultrafine-grained (UFG) samples. Compared with processing by HPT, subsequent processing by CR refines the crystallite size of all samples, increases the twin densities of UFG bronze and brass, and increases the dislocation density in UFG bronze. It also decreases the dislocation density in UFG brass and leads to an unchanged dislocation density in UFG copper. The results suggest there may be an optimum stacking fault energy for dislocation accumulation in UFG Cu–Zn alloys and this has important implications in the production of materials having reasonable strain hardening and good tensile ductility.

Keywords: Copper; Copper–zinc alloys; High-pressure torsion; Severe plastic deformation; Stacking fault energy; Ultrafine-grained materials

1. Introduction

Severe plastic deformation (SPD) is one of the most promising methods for fabricating bulk ultrafine-grained (UFG) materials for use in industrial applications [1]. During the SPD process, grain refinement is achieved by imposing very large strains in the samples through plastic deformation without any concomitant changes in their cross-sectional dimensions. It is well known that the plastic deformation of metallic materials depends upon dislocation slip and twinning as two of the primary deformation mechanisms. To date, most investigations have focused on grain refinement mechanisms in metals with relatively high values for the stacking fault energy (SFE) so that dislocation slips as the dominant deformation process [2–4]. For these metals, it was found that dislocation cell and/or low-angle grain boundaries (GBs) are first formed through dislocation accumulation at the beginning of the SPD process and additional deformation then transforms these interfaces into high-angle GBs through dislocation rearrangement and/or grain rotation. For metals and alloys having low values for the SFE, in which twinning may play a major and even dominant role in the plastic deformation, the grain refinement mechanism during SPD processing is not clearly defined. Nevertheless, there are some investigations showing that, when using the same SPD process, the material with a lower SFE may have a smaller grain size [5,6].

The UFG materials processed by SPD generally have high strength but relatively low ductility at ambient temperatures [7–9] where this low ductility is attributed to insufficient strain hardening due to an inability to accumulate dislocations [9–11]. For single-phase UFG materials where dislocation slip is the primary deformation mechanism, low ductility is usually reported except in a few isolated examples where excellent mechanical behavior was observed [12–17]. For UFG Cu–Zn alloys having different SFEs where twinning and/or twinning + dislocation slip dominate the plastic deformation, the most recent investigations show there is an optimum SFE that yields the optimum ductility [18,19]. It is reasonable to anticipate this effect arises

* Corresponding author. Tel.: +1 505 667 4029; fax: +1 505 667 2264.
E-mail address: yzhu@lanl.gov (Y.T. Zhu).

0921-5093/$ – see front matter © 2007 Elsevier B.V. All rights reserved.
doi:10.1016/j.msea.2007.06.014

because the UFG Cu–Zn alloy with an optimum SFE has the best capability for accumulating dislocations. When the stacking fault energy is too low, the grain size becomes too small after the same SPD processing and the stacking faults are saturated so that it is difficult to accumulate dislocations and deformation twins during subsequent tensile testing [19].

These results demonstrate the importance of studying the effect of the SFE, and therefore of the deformation mechanism, on the evolution of defect structures in UFG materials during further deformation. Accordingly, the present investigation was conducted in order to make use of X-ray diffraction (XRD) for an evaluation of the evolution of the defect structure in UFG Cu and Cu–Zn alloys processed by high-pressure torsion (HPT) and subsequently subjected to cold rolling (CR). The three materials of Cu, bronze (Cu–10 wt.% Zn) and brass (Cu–30 wt.% Zn) were used as model materials where these metals were selected because they have the same fcc single-phase crystal structure but different values for the SFE of 78, 35, and 14 mJ/m^2 [20–22], respectively.

2. Experimental materials and procedures

2.1. Sample preparation

Commercial copper (99.9% purity) and brass (Cu–30 wt.% Zn) were received in the form of rods with a diameter of 10 mm and bronze (Cu–10 wt.% Zn) was received in the form of plates with a thickness of 6 mm. These materials were sliced into disks with thicknesses of 0.8 mm and diameters of 10 mm for processing by HPT. The HPT was performed using a conventional processing facility in which the sample disk is placed between a stationary upper and a rotational lower Bridgman anvil [23]. Each disk was subjected to a total of five revolutions at room temperature using a rotation speed of 1 rotation/min with an imposed pressure of 6 GPa. The samples processed by HPT are henceforth designated the HPT samples.

To investigate the evolution of the defect structure in the HPT samples during subsequent deformation, some of the disks were processed by HPT and then cold-rolled into thin ribbons with a final thicknesses of ∼200 μm. The total thickness reduction for these samples was ∼75% after multiple rolling passes with a thickness reduction of ∼10% imposed in each separate pass. These samples are designated the HPT + CR samples.

2.2. X-ray diffraction

Quantitative X-ray diffraction measurements of the HPT and HPT + CR samples were performed using an X-ray diffractometer equipped with a Cu target operating at 1.8 kW and a graphite curved single-crystal ⟨0 0 0 2⟩ monochromator. The Cu Kα radiation was selected at the goniometer receiving slit section, the divergence and anti-scattering slits were set at 0.5° and 0.5°, respectively, and the width of the receiving slit was 0.3 mm. A series of θ–2θ scans was performed to provide a record of the XRD patterns at room temperature. Pure Al powder (99.999% purity) annealed at 200 °C in Ar was used as an XRD peak-broadening reference for both the grain size and the microstrain calculations. The peak parameters, including peak intensity, the peak-maximum position, the full width at half maximum and the integral breadth, were determined by fitting a Pearson VII function to the measured peaks. The XRD results were averaged from the whole disk/ribbon samples and they provide a representation of the defect structure information along the cross-sectional directions of the HPT and HPT + CR samples.

3. Experimental results

The XRD patterns of the HPT and HPT + CR samples are shown in Fig. 1(a) and (b), respectively. For the HPT samples, the HPT process introduced a {1 1 1} texture and the intensity of the texture decreased with decreasing SFE and therefore with increasing percentage of Zn in the Cu–Zn alloys. The CR process introduced an evident {1 1 0} rolling texture in which the intensity decreased with increasing Zn percentage. In addition, an increase in the Zn percentage in the Cu–Zn alloys led to a

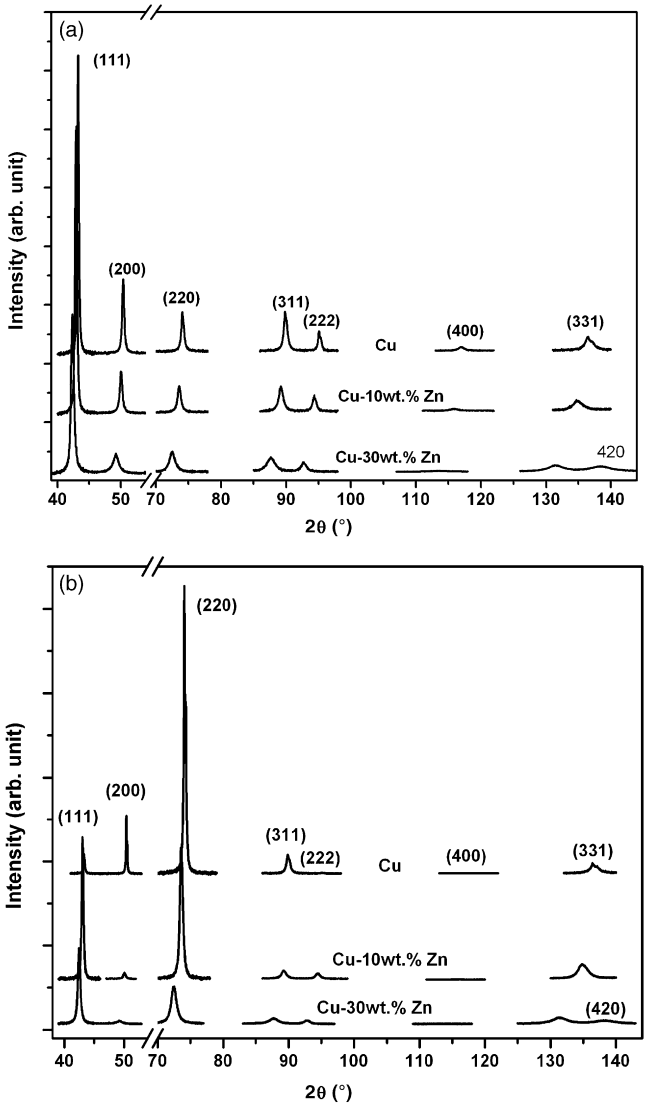

Fig. 1. XRD patterns for (a) HPT and (b) HPT + CR processed copper, bronze (Cu–10 wt.% Zn) and brass (Cu–30 wt.% Zn), respectively: the XRD peak indices are indicated.

Table 1
Lists of the XRD-measured average grain sizes and microstrains (d and $\langle\varepsilon^2\rangle^{1/2}$), grain sizes and microstrains (d_{111} and d_{200}, $\langle\varepsilon^2_{111}\rangle^{1/2}$ and $\langle\varepsilon^2_{200}\rangle^{1/2}$) along ⟨1 1 1⟩ and ⟨2 0 0⟩ directions, dislocation density (ρ), twin density (β), lattice parameters (a), absolute values of Burgers vectors (b), SFE (γ) [20–22] and shear modulus (G) [24] of HPT processed Cu, bronze (Cu–10 wt.% Zn) and brass (Cu–30 wt.% Zn): the errors of the XRD-measured grain sizes and microstrains are less than 20% and the errors of the lattice parameters are ∼0.0005 nm

Samples	Copper (99.9% Cu)	Bronze (Cu–10 wt.% Zn)	Brass (Cu–30 wt.% Zn)
d (nm)			
d_{111}	62	44	15
d_{200}	106	64	19
d	84	54	17
$\langle\varepsilon^2\rangle^{1/2}$ (%)			
$\langle\varepsilon^2_{111}\rangle^{1/2}$	0.11	0.12	0.38
$\langle\varepsilon^2_{200}\rangle^{1/2}$	0.17	0.20	0.70
$\langle\varepsilon^2\rangle^{1/2}$	0.14	0.16	0.54
ρ (10^{15} m^{-2})	0.24	0.40	4.22
β (%)	0.1	1.5	4.4
a (nm)	0.3619	0.3641	0.3691
b (nm)	0.2559	0.2575	0.2610
γ (mJ/m^2)	78	35	14
G (GPa)	48.3	46.5	40.1

shift in the XRD peaks towards lower diffraction angles. This was attributed to an increase in the lattice parameter due to the presence of the Zn solute, as listed in Tables 1 and 2.

3.1. Grain size and microstrain

Using the XRD peak broadening [25–27], it is possible to calculate the crystallite or coherent domain sizes and the microstrains of the HPT and HPT + CR samples. Because of the existences of {1 1 1} and {1 1 0} textures, it is possible in practice to calculate only the grain sizes (d_{111} and d_{200}) and the microstrains ($\langle\varepsilon^2_{111}\rangle^{1/2}$ and $\langle\varepsilon^2_{200}\rangle^{1/2}$) using the pairs of (1 1 1)–(2 2 2) and (2 0 0)–(4 0 0) reflections. The values of the mean crystallite size d and the microstrain $\langle\varepsilon^2\rangle^{1/2}$ were averaged from d_{111} and d_{200}, $\langle\varepsilon^2_{111}\rangle^{1/2}$ and $\langle\varepsilon^2_{200}\rangle^{1/2}$, respectively, and these mean values are listed in Tables 1 and 2 and depicted in Fig. 2(a) and (b), respectively.

As shown in Fig. 2(a), a decrease in SFE from 78 to 14 mJ/m^2, as in the transition from copper to brass, leads to a decrease in the average crystallite size from 84 to 17 nm for copper and brass, respectively, whereas the average microstrain increases from 0.13% in copper to 0.54% in brass. Moreover, it is readily apparent that the crystallite size and microstrain are anisotropic. For example, the value of d_{200} for UFG Cu processed by HPT (106 nm) is much larger than the value of d_{111} (62 nm) and in addition, the value of $\langle\varepsilon^2_{200}\rangle^{1/2}$ for the UFG brass processed by HPT (0.70%) is much larger than the value of $\langle\varepsilon^2_{111}\rangle^{1/2}$ (0.38%). Furthermore, Fig. 2(a) shows also that the difference between d_{111} and d_{200} decreases, while the difference between $\langle\varepsilon^2_{111}\rangle^{1/2}$ and $\langle\varepsilon^2_{200}\rangle^{1/2}$ increases, with a decreasing value in the SFE. For the UFG Cu–30 wt.% Zn processed by HPT, the value of d_{200} (19 nm) is very close to the value of d_{111} (15 nm) thereby indicating that equiaxed crystallites are formed in UFG brass with a low SFE.

Table 2
Lists of the XRD-measured average grain sizes and microstrains (d and $\langle\varepsilon^2\rangle^{1/2}$), grain sizes and microstrains (d_{111} and d_{200}, $\langle\varepsilon^2_{111}\rangle^{1/2}$ and $\langle\varepsilon^2_{200}\rangle^{1/2}$) along ⟨1 1 1⟩ and ⟨2 0 0⟩ directions, dislocation density (ρ), twin density (β), lattice parameters (a) and absolute values of Burgers vectors (b) of HPT + CR processed Cu, bronze (Cu–10 wt.% Zn) and brass (Cu–30 wt.% Zn): the errors of the XRD-measured grain sizes and microstrains are less than 20% and the errors of the lattice parameters are ∼0.0005 nm

Samples	Copper (99.9% Cu)	Bronze (Cu–10 wt.% Zn)	Brass (Cu–30 wt.% Zn)
d (nm)			
d_{111}	55	43	12
d_{200}	85	57	18
d	70	50	15
$\langle\varepsilon^2\rangle^{1/2}$ (%)			
$\langle\varepsilon^2_{111}\rangle^{1/2}$	0.08	0.16	0.25
$\langle\varepsilon^2_{200}\rangle^{1/2}$	0.16	0.28	0.45
$\langle\varepsilon^2\rangle^{1/2}$	0.12	0.22	0.35
ρ (10^{15} m^{-2})	0.23	0.59	3.10
β (%)	0.1	4.8	8.0
a (nm)	0.3617	0.3640	0.3690
b (nm)	0.2558	0.2574	0.2609

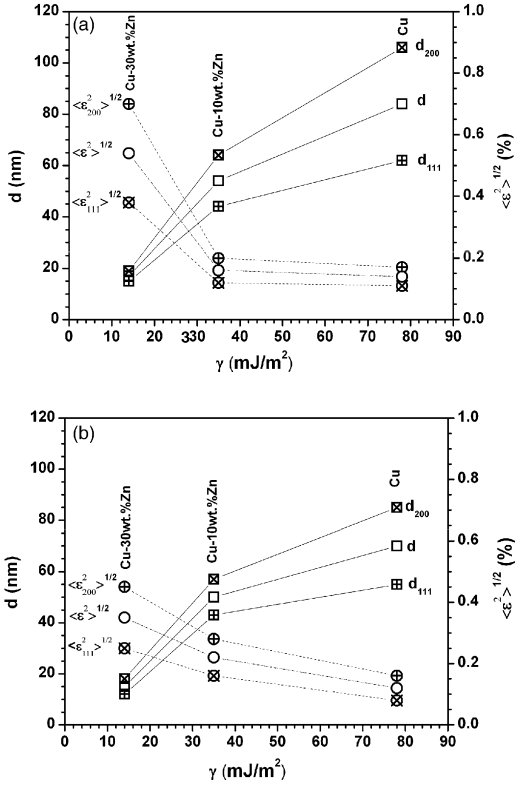

Fig. 2. XRD-measured average crystallite sizes and microstrains (d and $\langle\varepsilon^2\rangle^{1/2}$) and the crystallite sizes and microstrains (d_{111} and d_{200}, $\langle\varepsilon^2_{111}\rangle^{1/2}$ and $\langle\varepsilon^2_{200}\rangle^{1/2}$) along ⟨1 1 1⟩ and ⟨2 0 0⟩ directions for (a) HPT and (b) HPT + CR processed copper, bronze (Cu–10 wt.% Zn) and brass (Cu–30 wt.% Zn), respectively: the errors of the XRD-measured grain sizes and microstrains are less than 20%.

Fig. 2(b) shows that processing by CR does not affect either the variation trends of the crystallite sizes and microstrains or the extent of the anisotropy with respect to the SFE. Thus, a decrease in the SFE leads to a corresponding decrease in the crystallite size and its anisotropy as well as an increase in the microstrain and its anisotropy. This result further confirms the influence of the SFE on the crystallite size and microstrain under the same deformation strain. Nevertheless, the CR process further refined the crystallites of all three samples and it is apparent from inspection of Tables 1 and 2 that this crystallite refinement decreases with decreasing SFE. More importantly, the CR process leads to a decrease in the microstrains of UFG Cu and brass from 0.14 to 0.12% and 0.54 to 0.35%, respectively, while processing by CR increases the microstrain of UFG bronze from 0.16 to 0.22%.

3.2. The dislocation and twin densities

The dislocation density ρ, may be calculated from the crystallite size d, and microstrain, $\langle\varepsilon^2\rangle^{1/2}$, measured by XRD using the relationship [28–31]:

$$\rho = \frac{2\sqrt{3}\langle\varepsilon^2\rangle^{1/2}}{d_{\mathrm{XRD}}b} \quad (1)$$

where b is the absolute value of the Burgers vector which for fcc metals, is the length of a unit dislocation along the $\langle 1\,1\,0\rangle$ direction so that $b = (\sqrt{2}/2)a$ where a is the lattice parameter. The calculated values of ρ and b and the appropriate values of a are listed for the HPT and HPT + CR samples in Tables 1 and 2, respectively. The twin density β, defined as the probability of finding a twin boundary between any two neighboring $\{1\,1\,1\}$ planes, was calculated using the expression [32,33]:

$$\beta = \frac{\Delta\mathrm{C.G.}(2\theta)_{1\,1\,1} - \Delta\mathrm{C.G.}(2\theta)_{2\,0\,0}}{11\tan\theta_{1\,1\,1} + 14.6\tan\theta_{2\,0\,0}} \quad (2)$$

where ΔC.G.$(2\theta)_{111}$ and ΔC.G.$(2\theta)_{200}$ are the angular deviations of the gravity center from the peak maximum of the $\{1\,1\,1\}$ and $\{2\,0\,0\}$ XRD peaks, respectively. In practice, Eq. (2) provides only a qualitative estimate of the twin density because it is known that the asymmetry of the XRD peaks may be affected by several other features in addition to twinning [34].

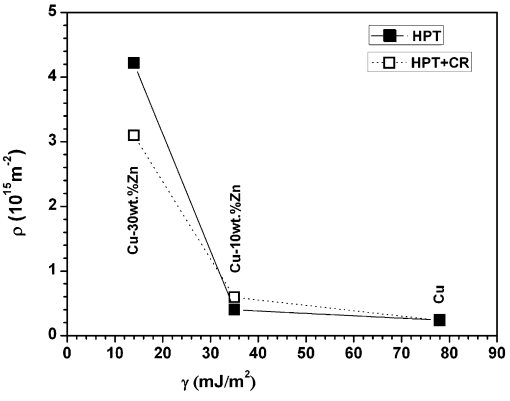

Fig. 3. Dislocation densities ρ, in HPT and HPT + CR processed copper, bronze (Cu–10 wt.% Zn) and brass (Cu–30 wt.% Zn).

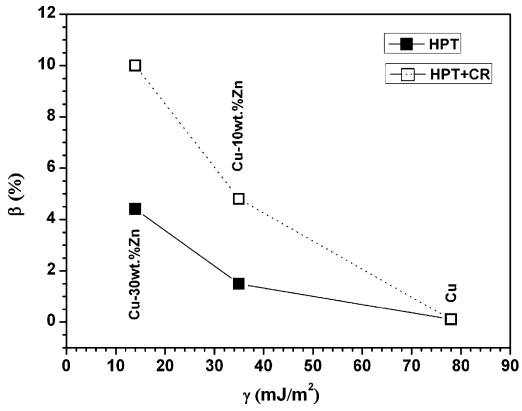

Fig. 4. Twin densities β, in HPT and HPT + CR processed copper, bronze (Cu–10 wt.% Zn) and brass (Cu–30 wt.% Zn).

As listed in Tables 1 and 2 and shown in Fig. 3 for both the HPT and HPT + CR samples, the dislocation density increases with decreasing SFE. For example, the dislocation density of the HPT samples increases from $0.20 \times 10^{15}\,\mathrm{m}^{-2}$ for copper to $4.22 \times 10^{15}\,\mathrm{m}^{-2}$ for brass when the SFE decreases from 78 to 14 mJ/m^2, respectively. Moreover, the CR process significantly increases the dislocation density in the UFG bronze from 0.40×10^{15} to $0.59 \times 10^{15}\,\mathrm{m}^{-2}$ while at the same time maintaining an essentially constant value for ρ in UFG copper where the values are $0.24 \times 10^{15}\,\mathrm{m}^{-2}$ for the HPT process and $0.23 \times 10^{15}\,\mathrm{m}^{-2}$ for the HPT + CR process and, in addition, decreasing the value of ρ in UFG brass from 4.22×10^{15} to $3.10 \times 10^{15}\,\mathrm{m}^{-2}$. These measurements show that the CR process gives rise to dislocation recovery in UFG brass while introducing more dislocations in UFG bronze.

As shown in Fig. 4, a decrease in the SFE leads to an increase in the twin density for both the HPT and the HPT + CR samples. For the HPT samples, the twin density increases from 0.1 to 4.4% when the SFE decreases from 78 to 14 mJ/m^2 for copper and brass, respectively. However, the CR process does not change the twin density in UFG copper although it increases the twin densities in UFG bronze and brass from 1.5 to 4.8% and 4.4 to 8.0%, respectively. Thus, the increase in the twin density with processing by CR increases with decreasing SFE.

4. Discussion

4.1. Grain size and microstrain

It is important to note that the crystallite sizes of the HPT + CR samples measured by XRD are smaller than the grain sizes measured by transmission electron microscopy (TEM). For example, the measured TEM grain sizes in the middle positions of UFG copper and bronze ribbons processed by HPT + CR are 180 and 110 nm, respectively [6]. This difference arises because the XRD process determines the size of the coherent diffraction domains and this includes both the subgrains and the dislocation cells [2]. However, the measured XRD grain sizes of the whole HPT disks are slightly larger than the TEM values at the edges of the disks, which are 75, 50 and 10 nm, respectively for copper, bronze and brass [5], because of the inhomogeneous grain size

distribution of the HPT processed disk from the disk edge to center.

The data from XRD indicate that a decrease in the SFE leads to a decrease in the crystallite size for the HPT and HPT + CR samples. This can be explained qualitatively by noting that a lower SFE promotes deformation twinning and this is conducive to promoting additional grain refinement. Moreover, a lower value of the SFE increases the difficulty for dissociated dislocations to recombine and cross-slip thereby impeding the dislocation recovery process and consequently leading to a smaller grain size.

An important theoretical model was developed recently by Mohamed [35] to predict the minimum grain size of nanocrystalline metals processed by ball milling. This model essentially characterizes the microstructure through the structural decomposition of an array of large grains due to the imposition of severe plastic deformation. Since the model is based explicitly on the effect of processing by SPD and the consequent introduction of large strains, it is reasonable to anticipate the model will be equally applicable to other types of SPD processing including HPT and CR. According to the model [35], the measured minimum grain size $d_{\min}$, is related to the SFE γ, through a relationship of the form:

$$\frac{d_{\min}}{b} = A\left(\frac{\gamma}{Gb}\right)^{q} \tag{3}$$

where A is a constant and G is the shear modulus. The values of γ [20–22] and G [24] for copper, bronze and brass are listed in Table 1. According to the theory, the value of the exponent of the normalized SFE is given by $q = 0.5$.

Fig. 5 shows a plot of $\ln(d_{\min}/b)$ versus $\ln(\gamma/Gb)$ using the XRD and TEM [5,6] data. It is apparent that the data from UFG copper and UFG bronze lead to exponents for the normalized SFE within the range of ~0.45 to ~0.64. Thus, these values of q are close to the value of ~0.65 derived from earlier results

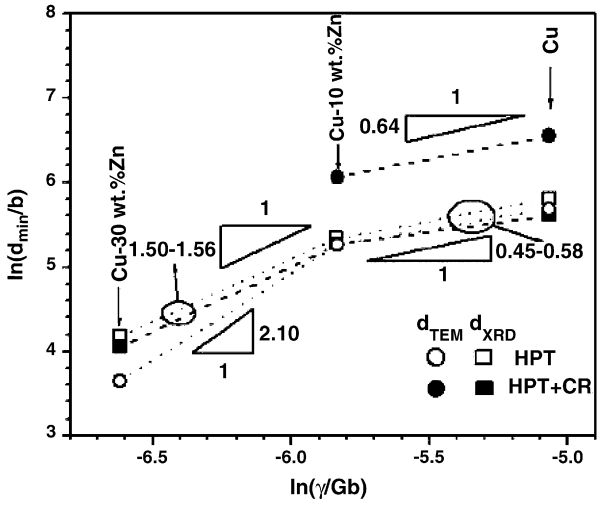

Fig. 5. Plot of $\ln(d_{\min}/b)$ vs. $\ln(\gamma/Gb)$ showing data for UFG copper and bronze lead to exponents for the normalized SFE within the range of ~0.45–0.64 and data for UFG brass deviate downwards yielding exponents for the normalized SFE within the range of ~1.50–2.10. The measured TEM grain sizes of HPT and HPT + CR samples were reported earlier [5,6].

reported by Mohamed [35] and they are also supportive of the theoretical model where the value of q is 0.5. However, the experimental data from UFG brass deviate downwards from the lines for UFG copper and UFG bronze thereby yielding higher exponents for the normalized SFE within the range of ~1.50–2.10. It is apparent that these values are significantly higher than the value predicted by the theoretical model. To resolve this apparent dichotomy, it is important to note that high-resolution TEM has revealed the presence of an amorphous layer along the GBs of the HPT and HPT + CR processed brass [5,19] and this suggests that UFG brass deforms not only by twinning and dislocation slip but also by GB sliding. The occurrence of GB sliding probably further reduces the minimum grain size thereby leading to a deviation from the slope predicted by the theoretical model.

4.2. The twin and dislocation densities

The results show the twin density increases with decreasing SFE in both the HPT and HPT + CR samples and this trend is a direct consequence of the lower SFE, which makes the formation of deformation twins significantly easier. The twin density of the UFG copper processed by HPT is very low and the additional processing by the CR process has no significant effect because the SFE of Cu is relatively high and the primary deformation mode at room temperature is dislocation slip. The increase in the twin density in UFG bronze and UFG brass through processing by CR suggests the twin density was probably not saturated after HPT and therefore it increases with further deformation. Thus, the deformation mechanisms in brass and bronze include both twinning and dislocation slip and the newly formed twins developed during CR lead to additional grain refinement in UFG brass and bronze.

There is a simple explanation for the increase in the dislocation density with decreasing SFE in the HPT and HPT + CR samples. First, the reduction in the SFE promotes the splitting of the full dislocations into two partials containing a wide stacking fault ribbon. This splitting makes it difficult for the dislocation to cross-slip or climb when it encounters a barrier, thereby hindering these two potential recovery mechanisms. This means that a reduction in the SFE usually leads to a higher dislocation density. Second, a lower SFE also promotes the formation of deformation twins. Experiments on Cu showed recently that boundaries of both growth and deformation twins may act as locations for dislocation accumulation and this also increases the dislocation density [15–17]. Therefore, the high-twin density in UFG bronze and brass should assist in raising their dislocation densities.

The lack of any significant change in the dislocation density in UFG copper during processing by CR probably reflects the presence of saturation in the dislocation density after processing by HPT. This means in practice that processing by CR is unable to further increase the dislocation density due to the dynamic equilibrium between dislocation formation and annihilation.

As already demonstrated, a high twin density usually leads to a high dislocation density. Therefore, the increase in the twin density in UFG brass and bronze during CR should promote an increase in the dislocation density. In practice, however, this was not the case for UFG brass where the dislocation density

decreased during processing by CR. The reason for this reduction is not fully understood at the present time and this trend requires additional investigations using high-resolution TEM. By contrast, the increased dislocation density in UFG bronze during processing by CR is due primarily to the increased twin and stacking fault density. These results suggest, therefore, there is an optimum SFE which leads in subsequent processing by CR, to a maximum accumulation of dislocations and hence this optimum condition provides the capability of attaining reasonable strain hardening and good tensile ductilities in tests conducted at ambient temperatures.

Finally, it should be pointed out that the XRD peak analysis, used in this investigation to calculate the grain size and microstrain/dislocation density, is a simplified method. It does not take into consideration some detailed structural parameters such as the presence of twins, the anisotropies of grain shape, etc. Recently, a modified XRD peak broadening method was introduced [36–38] and a recent report described the use of this procedure for measuring mean grain sizes [39].

5. Summary and conclusions

1. Investigations by X-ray diffraction using samples of copper, bronze and brass processed by high-pressure torsion (HPT) and by HPT with subsequent cold rolling (CR) indicate that a reduction in the stacking fault energy leads to both a decrease in the crystallite size and an increase in the dislocation and twin densities.
2. When samples processed by HPT are further processed by CR, there is a reduction in the crystallite size in ultrafine-grained (UFG) copper, bronze and brass, an increase in the twin density in UFG bronze and brass, an increase in the dislocation density in UFG bronze but a decrease in the dislocation density in UFG copper and brass. These results are reasonably explained based on a consideration of the dominant deformation mechanisms.
3. The results for UFG copper and bronze show reasonable consistency with a theoretical model predicting the minimum grain size produced through processing using severe plastic deformation but there is a deviation from the model for UFG brass.
4. The results suggest there is an optimum stacking fault energy for dislocation accumulation in UFG Cu–Zn alloys and it is reasonable to anticipate this optimum condition will yield good strain hardening and tensile ductility.

References

[1] R.Z. Valiev, Y. Estrin, Z. Horita, T.G. Langdon, M.J. Zehetbauer, Y.T. Zhu, JOM 58 (4) (2006) 33.
[2] Y.T. Zhu, J.Y. Huang, J. Gubicza, T. Ungár, Y.M. Wang, E. Ma, R.Z. Valiev, J. Mater. Res. 18 (2003) 1908.
[3] S.V. Dobatkin, E.N. Bastarache, G. Sakai, T. Fujita, Z. Horita, T.G. Langdon, Mater. Sci. Eng. A 408 (2005) 141.
[4] N.R. Tao, Z.B. Wang, W.P. Tong, M.L. Sui, J. Lu, K. Lu, Acta Mater. 50 (2002) 4603.
[5] Y.H. Zhao, X.Z. Liao, Y.T. Zhu, Z. Horita, T.G. Langdon, Mater. Sci. Eng. A 410–411 (2005) 188.
[6] Y.H. Zhao, X.Z. Liao, Y.T. Zhu, Z. Horita, T.G. Langdon, Mater. Sci. Eng. A 463 (2007) 22.
[7] C.C. Koch, Scripta Mater. 49 (2003) 657.
[8] D. Jia, Y.M. Wang, K.T. Ramesh, E. Ma, Y.T. Zhu, R.Z. Valiev, Appl. Phys. Lett. 79 (2001) 611.
[9] Y.T. Zhu, X.Z. Liao, Nature Mater. 3 (2004) 351.
[10] H. Van Swygenhoven, J.R. Weertman, Scripta Mater. 49 (2003) 625.
[11] Z. Budrovic, H. Van Swygenhoven, P.M. Derlet, S.V. Petegem, B. Schmitt, Science 304 (2004) 273.
[12] R.Z. Valiev, I.V. Alexandrov, Y.T. Zhu, T.C. Lowe, J. Mater. Res. 17 (2002) 5.
[13] K.M. Youssef, R.O. Scattergood, K.L. Murty, J.A. Horton, C.C. Koch, Appl. Phys. Lett. 87 (2005) 091904.
[14] H.W. Höppel, J. May, M. Göken, Adv. Eng. Mater. 6 (2004) 781.
[15] L. Lu, Y. Shen, X. Chen, L. Qian, K. Lu, Science 304 (2004) 422.
[16] E. Ma, Y.M. Wang, Q.H. Lu, M.L. Sui, L. Lu, K. Lu, Appl. Phys. Lett. 85 (2004) 4932.
[17] Y.H. Zhao, J.F. Bingert, X.Z. Liao, B.Z. Cui, K. Han, A. Sergueeva, A.K. Mukherjee, R.Z. Valiev, T.G. Langdon, Y.T. Zhu, Adv. Mater. 18 (2006) 2949.
[18] Y.H. Zhao, Y.T. Zhu, X.Z. Liao, Z. Horita, T.G. Langdon, Appl. Phys. Lett. 89 (2006) 121906.
[19] Y.H. Zhao, X.Z. Liao, Z. Horita, T.G. Langdon, Y.T. Zhu, Mater. Sci. Eng. A, submitted for publication.
[20] P.C.J. Gallagher, Met. Trans. 1 (1970) 2429.
[21] M.H. Loretto, L.M. Clarebrough, R.L. Segall, Phil. Mag. 11 (1965) 459.
[22] A. Howie, P.R. Swann, Phil. Mag. 6 (1961) 1215.
[23] G. Sakai, Z. Horita, T.G. Langdon, Mater. Sci. Eng. A 393 (2005) 344.
[24] E.A. Brandes, G.B. Brook, Smithells Metals Reference Book, 7th ed., Butterworth–Heinemann Ltd., Oxford, 1992, p. 15.
[25] H.P. Klug, L.E. Alexander, X-ray Diffraction Procedures for Polycrystalline and Amorphous Materials, 2nd ed., Wiley, New York, 1974, p. 49, (Chapter 9).
[26] Y.H. Zhao, K. Zhang, K. Lu, Phys. Rev. B 56 (1997) 14322.
[27] Y.H. Zhao, H.W. Sheng, K. Lu, Acta Mater. 49 (2001) 365.
[28] G.K. Williamson, R.E. Smallman, Phil. Mag. 1 (1956) 34.
[29] R.E. Smallman, K.H. Westmacott, Phil. Mag. 2 (1957) 669.
[30] Y.H. Zhao, K. Lu, K. Zhang, Phys. Rev. B 66 (2002) 085404.
[31] Y.H. Zhao, X.Z. Liao, Z. Jin, R.Z. Valiev, Y.T. Zhu, Acta Mater. 52 (2004) 4589.
[32] J.B. Cohen, C.N.J. Wagner, J. Appl. Phys. 33 (1962) 2073.
[33] C.N.J. Wagner, Acta Metall. 5 (1957) 427.
[34] T. Ungar, Scripta Mater. 51 (2004) 777.
[35] F.A. Mohamed, Acta Mater. 51 (2003) 4107.
[36] T. Ungar, J. Gubicza, G. Ribarik, A. Borbely, J. Appl. Cryst. 34 (2001) 298.
[37] G. Ribarik, N. Audebrand, H. Palancher, T. Ungar, D. Louer, J. Appl. Cryst. 38 (2005) 912.
[38] L. Balogh, G. Ribarik, T. Ungar, J. Appl. Phys. 100 (2006) 023512.
[39] T. Ungar, L. Balogh, Y.T. Zhu, Z. Horita, C. Xu, T.G. Langdon, Mater. Sci. Eng. A 444 (2007) 153.